Human Molecular Genetics, 2012, Vol. 21, No. 17 ***3785–3794***
doi:10.1093/hmg/dds206
Advance Access published on May 29, 2012

Identification of novel ATP13A2 interactors and their role in α-synuclein misfolding and toxicity

Marija Usenovic[1,2], Adam L. Knight[3], Arpita Ray[3], Victoria Wong[4], Kevin R. Brown[5], Guy A. Caldwell[3,6], Kim A. Caldwell[3,6], Igor Stagljar[4] and Dimitri Krainc[1,*]

[1]Department of Neurology, Massachusetts General Hospital, Harvard Medical School, MassGeneral Institute for Neurodegenerative Disease, Charlestown, MA 02129, USA, [2]Mediterranean Institute for Life Sciences, Split 21000, Croatia, [3]Department of Biological Sciences, The University of Alabama, Tuscaloosa, AL 35487, USA, [4]Department of Biochemistry and Department of Molecular Genetics and [5]Banting and Best Department of Medical Research, Donnelly Centre, University of Toronto, Toronto, ON, Canada M5S 3E1 and [6]Departments of Neurology and Neurobiology, Center for Neurodegeneration and Experimental Therapeutics, University of Alabama at Birmingham, Birmingham, AL 35294, USA

Received March 1, 2012; Revised and Accepted May 23, 2012

Lysosomes are responsible for degradation and recycling of bulky cell material, including accumulated misfolded proteins and dysfunctional organelles. Increasing evidence implicates lysosomal dysfunction in several neurodegenerative disorders, including Parkinson's disease and related synucleinopathies, which are characterized by the accumulation of α-synuclein (α-syn) in Lewy bodies. Studies of lysosomal proteins linked to neurodegenerative disorders present an opportunity to uncover specific molecular mechanisms and pathways that contribute to neurodegeneration. Loss-of-function mutations in a lysosomal protein, ATP13A2 (PARK9), cause Kufor–Rakeb syndrome that is characterized by early-onset parkinsonism, pyramidal degeneration and dementia. While loss of ATP13A2 function plays a role in α-syn misfolding and toxicity, the normal function of ATP13A2 in the brain remains largely unknown. Here, we performed a screen to identify ATP13A2 interacting partners, as a first step toward elucidating its function. Utilizing a split-ubiquitin membrane yeast two-hybrid system that was developed to identify interacting partners of full-length integral membrane proteins, we identified 43 novel interactors that primarily implicate ATP13A2 in cellular processes such as endoplasmic reticulum (ER) translocation, ER-to-Golgi trafficking and vesicular transport and fusion. We showed that a subset of these interactors modified α-syn aggregation and α-syn-mediated degeneration of dopaminergic neurons in *Caenorhabditis elegans*, further suggesting that ATP13A2 and α-syn are functionally linked in neurodegeneration. These results implicate ATP13A2 in vesicular trafficking and provide a platform for further studies of ATP13A2 in neurodegeneration.

INTRODUCTION

Lysosomes are part of essential cellular pathways responsible for the degradation and recycling of bulky cell material and maintaining cellular homeostasis. Dysfunction of proteins involved in lysosomal regulation or function results in the accumulation of undigested material that can disturb other cellular processes, including autophagy, endocytosis and exocytosis, lysosomal pH regulation, vesicle maturation, synaptic release and calcium homeostasis (1). Increasing evidence implicates lysosomal dysfunction in a wide array of neurodegenerative disorders (2,3). Neurons appear to be particularly vulnerable to lysosomal impairment, since most of the diseases characterized by lysosomal dysfunction also exhibit neurodegeneration (1). Neurodegenerative disorders that are caused by mutations of

*To whom correspondence should be addressed at: Department of Neurology, Massachusetts General Hospital, Harvard Medical School, MassGeneral Institute for Neurodegenerative Disease, 114 16th Street, Room 2008, Charlestown, MA 02129, USA. Tel: +1 6177241726; Fax: +1 6177241480; Email: krainc@helix.mgh.harvard.edu

integral lysosomal proteins present an opportunity to elucidate specific molecular mechanisms and pathways that contribute to neurodegeneration (1,2).

Mutations in lysosomal ATP13A2 (PARK9) have been recently identified as the cause of Kufor–Rakeb syndrome that is characterized by juvenile parkinsonism, pyramidal degeneration and dementia (4–6). Moreover, ATP13A2 plays a role in α-syn misfolding and toxicity in yeast and *Caenorhabditis elegans* models of Parkinson's disease (PD) (7–9). Recent data also implicate loss of ATP13A2 function in mitochondrial maintenance and oxidative stress, lending further support to the importance of lysosomes for mitochondrial quality control (10,11).

The role of normal ATP13A2 in the central nervous system is not known, but it is predicted to function as a lysosomal P5-type ATPase that regulates cation homeostasis (12,13). Here, we screened a human brain cDNA library to identify ATP13A2 interacting partners as a first step toward elucidating its function. Using the split-ubiquitin (Ub) membrane yeast two-hybrid (MYTH) system developed to identify interacting partners of integral membrane proteins (14), we identified 43 interactors that suggest the involvement of ATP13A2 in vesicular trafficking. Moreover, we found that a subset of these interacting proteins modifies α-syn aggregation and neurotoxicity in *C. elegans*, further strengthening the functional link between ATP13A2 and synucleinopathies.

RESULTS

Novel interacting proteins of ATP13A2 identified by MYTH screening

Since ATP13A2 is a transmembrane protein, we utilized a yeast two-hybrid system specifically designed to identify interactors of membrane proteins (14,15). This method, the split-Ub MYTH system, entails the reassociation of two Ub halves by specific protein–protein interactions (16). The protein of interest (bait) is fused in its full-length form to a C-terminal fragment of Ub (Cub), followed by an artificial transcription factor (TF). The putative interactor (prey) is fused to the N-terminal fragment of Ub carrying an Ile13Gly mutation (NubG). If the bait and prey interact, an active Ub molecule is reconstituted. This is recognized by cytoplasmic Ub proteases that cause the proteolytic cleavage of the TF, allowing its translocation to the nucleus and activation of yeast reporter genes, resulting in growth of yeast on selective media (14,15,17) (Fig. 1A).

One of the prerequisites for a successful MYTH screen is to establish that the full-length bait protein gets correctly expressed and targeted to its membrane compartment, but does not self-activate the reporter genes in the presence of a non-specific interacting protein. To this end, the bait construct ATP13A2-Cub-TF was tested on selective media in the presence of two commonly used non-interacting yeast integral membrane proteins, Ost1 [a component of the oligosaccharyltransferase complex in the endoplasmic reticulum (ER) membrane] and Fur4 (an uracil permease localized to the plasma membrane). These two proteins were fused to NubI (Ost1-NubI or Fur4-NubI). NubI positive control constructs activate the yeast reporter system independently of a bait protein interaction, because of high affinity of NubI (the wild-type form of N terminus half of Ub) for Cub, resulting in active Ub molecules (17). Activation of the reporter system in yeast cells co-expressing ATP13A2-Cub-TF and either of the NubI positive controls indicated that the bait protein was expressed, correctly inserted into the membrane, and the TF properly cleaved upon the formation of active Ub (Supplementary Material, Fig. S1). As an additional control, the same two non-interacting yeast membrane proteins (Ost1 and Fur4) were fused to mutant NubG (Ost1-NubG or Fur4-NubG). These constructs served as negative controls, since they should not interact with the human ATP13A2 bait fused to Cub. Lack of growth of yeast cells co-expressing ATP13A2-Cub-TF and non-interacting control prey (Ost1-NubG or Fur4-NubG) indicated that the bait construct was not self-activating (Supplementary Material, Fig. S1).

Following confirmation that the ATP13A2 bait protein was suitable for MYTH, we performed a large-scale screen using a human brain library with cDNAs fused C-terminally to the NubG moiety (DualSystems Biotech Inc., Zurich, Switzerland).

From a screen of $\sim 4 \times 10^6$ yeast transformants, 43 novel ATP13A2 interactors were identified (Supplementary Material, Table S1, Fig. 2A). These interactors were specific because they only interacted with ATP13A2 bait (Fig. 1B), but not with the artificial bait construct MFα-CD4-Cub-TF (Fig. 1C). Prey candidates that activate the reporter system in the presence of the artificial bait are considered spurious because they activate the reporter system in a manner independent of bait identity (15,18). As shown in Figure 1B, yeast cells were selected for growth on selective medium (SD-Trp-Leu), confirming the presence of both ATP13A2 bait and prey vectors, and for growth and development of blue color on X-gal medium (SD-Trp-Leu-Ade-His + X-gal) confirming the interactions. Yeast cells expressing artificial bait and prey that did not grow on the same selective media were considered specific interactors (Fig. 1C).

A subset of these prey candidates was then reconfirmed as ATP13A2 interactors by co-immunoprecipitation (Fig. 1D). Based on the availability of constructs, we selected seven candidates and expressed them together with V5-tagged ATP13A2 in HEK293 cells. Using immunoprecipitation of whole cell lysates with V5 antibody, we reconfirmed all seven proteins as ATP13A2 interacting partners [histone deacetylase 6 (HDAC6), NIX (also named BNIP3L), heat shock 70 kDa protein 8 (HSPA8), synaptotagmin 11, G-associated kinase (GAK), adaptor-associated kinase 1 (AAK1) and Yip1 interacting factor homolog A (YIF1A)], validating the reliability of the MYTH method.

Functional assignment of MYTH data

In order to examine the functions of the ATP13A2 interactors, gene ontology (GO) terms were used to group the interactors based on their biological annotations (19). First MYTH-identified interactors with related GO terms were visualized as a network (Fig. 2A), combined with known and predicted interactions from two online databases (see Materials and Methods). This network demonstrates that few interactions were previously known among the bait and 43 interactors and that the hit proteins provide functional genetic links

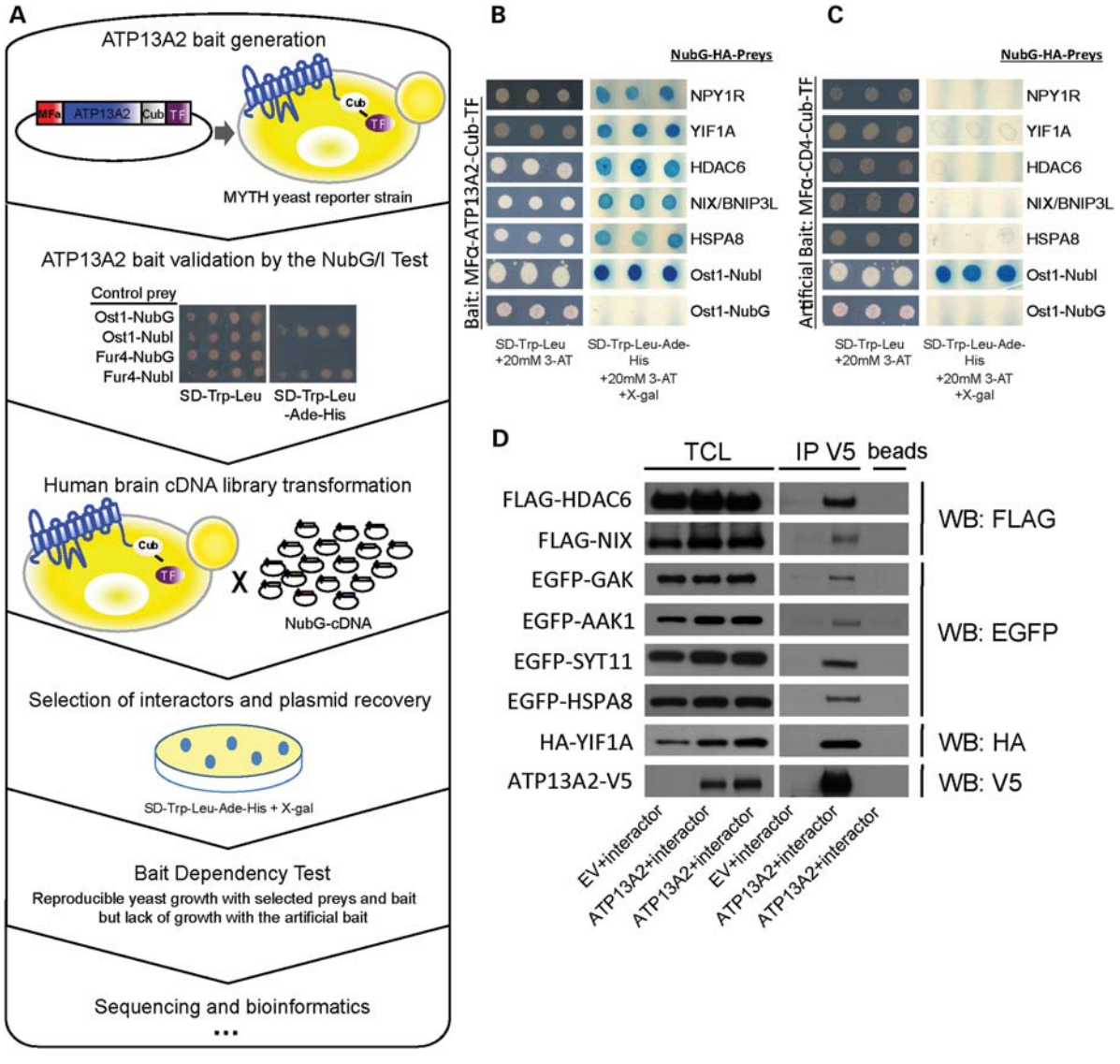

Figure 1. Verification of ATP13A2 interactors. (**A**) Flowchart of MYTH describing general steps to identify interactors of membrane-based proteins. The ATP13A2 bait was generated and tested for expression and self-activation of reporter genes by the 'NubG/I test' which uses negative and positive control preys; cDNA library was introduced in the ATP13A2-Cub-TF expressing yeast strain and putative interactors were selected on selective media; prey plasmids were extracted and amplified. A 'bait dependency test', which employs an artificial bait protein, was used to identify spurious preys and to finalize a list of interactors that were sequenced and further analyzed. (**B**) Representative pictures of yeast strain THY.AP40 containing interacting bait–prey pairs grown on selective plates with X-gal. (**C**) The specificity of the interactions was determined with a bait dependency test using the artificial bait construct MFα-CD4-Cub-TF as a negative control. Yeast strain THY.AP40 carrying this artificial bait was transformed with the same NubG-hemagglutinin (HA) preys used in the screen in (B). Interactors incapable of non-specifically activating the reporter system in this strain were considered for further analysis. To confirm the correct expression and lack of self-activation of both bait and artificial bait constructs, Ost1-NubI and Ost1-NubG were used as positive and negative controls, respectively. Selection medium was supplemented with 20 mM 3-AT to increase the stringency of the selection. (**D**) Co-immunoprecipitation of HEK293FT cells co-transfected with ATP13A2-V5 and selected interactors. Cell lysates were immunoprecipitated (IP) with V5 antibody that recognizes tagged ATP13A2-V5. Samples were immunoblotted and probed with antibodies against tags of the constructs carrying the indicated protein. In each case, the proteins of interest were fused at the N terminus with epitope tags [FLAG, enhanced green fluorescence protein, HA, as labeled], except the ATP13A2 that had the V5 tag on C terminus. Specificity of the interaction between the candidates and ATP13A2 can be observed by comparing total cell lysate (TCL) lanes with the immunoprecipitation lanes (IP V5, beads). EV, empty vector.

from ATP13A2 to protein transport, vesicle trafficking, cell adhesion and cell fate.

Additionally, we used a functional annotation tool (DAVID) that clusters related GO terms and provides a score representing enrichment (20).

This analysis resulted in 18 clusters (Fig. 2B; see Supplementary Material, Table S2, for a complete list of clusters of GO terms) with one of the top scoring clusters (referred to as ER in Fig. 2B) that included proteins involved in ER transport, ER-to-Golgi trafficking and protein folding [SEC61B, HSPA8, LMAN2, YIF1A, FK506-binding protein 8 (FKBP38), PDIA6, SPCS2, UBE2J2, LRP6].

Other notable functional categories included clathrin-mediated endocytosis (HSPA8, GAK, AAK1), vesicular

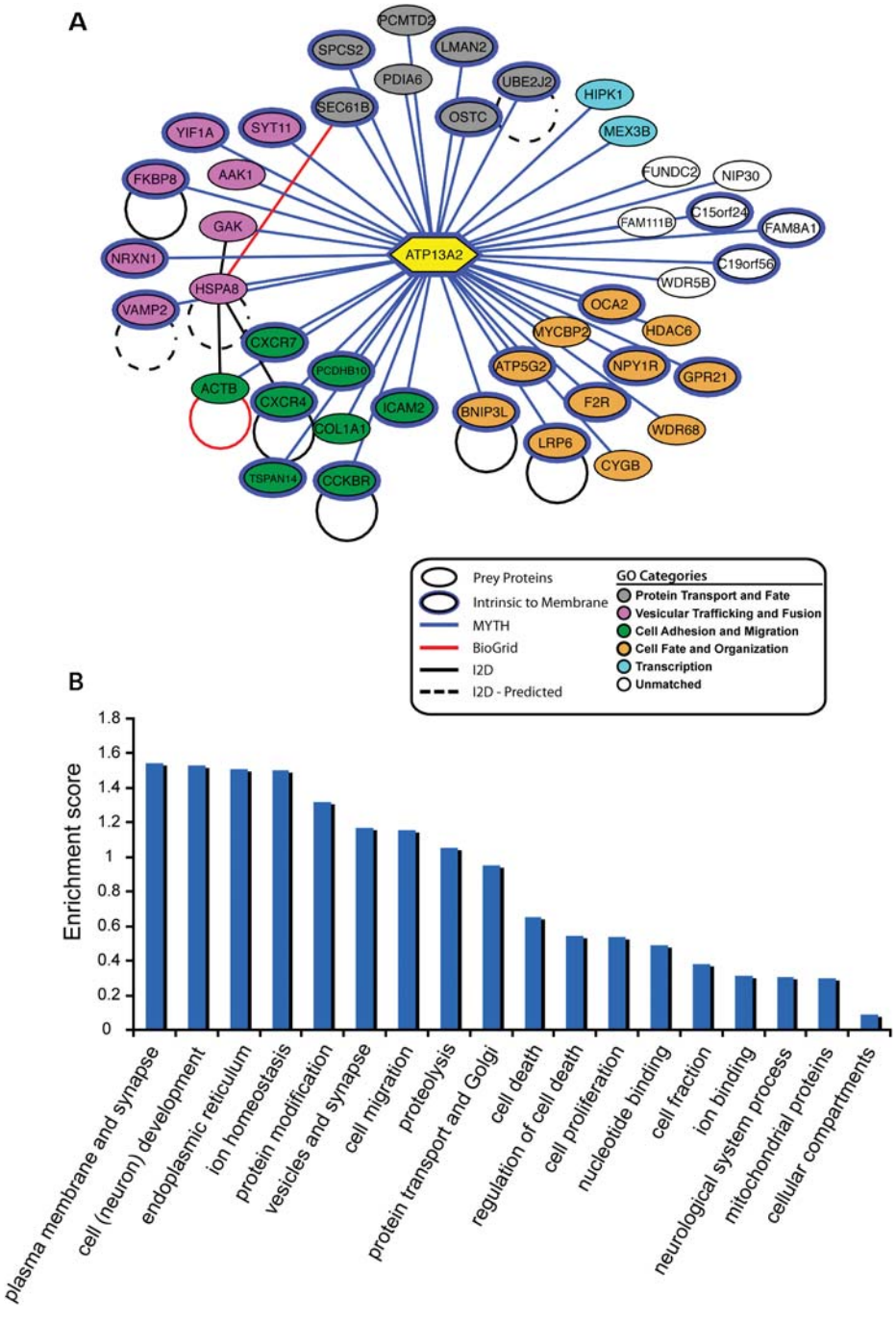

Figure 2. Functional assignment of ATP13A2 interactors. (**A**) The interactome of ATP13A2 identified using the MYTH technology was visualized using the NAViGaTOR graph visualization software. Edges indicate the source of interaction data, while the node colors reflect manual assignment of each gene into functional categories based on GO annotations (see Materials and Methods). Blue node highlights indicate genes annotated by GO to be intrinsic to the plasma membrane. (**B**) Graph represents clusters of GO terms obtained by a DAVID functional annotation tool.

trafficking and fusion [SYT11, vesicle-associated membrane protein 2 (VAMP2), NRXN1] and cell migration and adhesion (CXCR4, CXCR7, ICAM2 and PCDHB10). Also, the fourth-highest scoring cluster is consisted of interactors involved in ion homeostasis (CXCR4, NPY1R, F2R, CCKBR), emphasizing the previously suggested involvement of ATP13A2 in cation homeostasis (8,13,21). The prominence of cellular processes such as ER translocation, ER-to-Golgi trafficking, vesicular transport and fusion in this analysis suggested the involvement of ATP13A2 in vesicular trafficking.

Deficiency of ATP13A2 interactors exacerbates α-syn misfolding in *C. elegans*

ATP13A2 was recently identified as a modifier of α-syn toxicity and misfolding in yeast (8,9) and *C. elegans* (9,10).

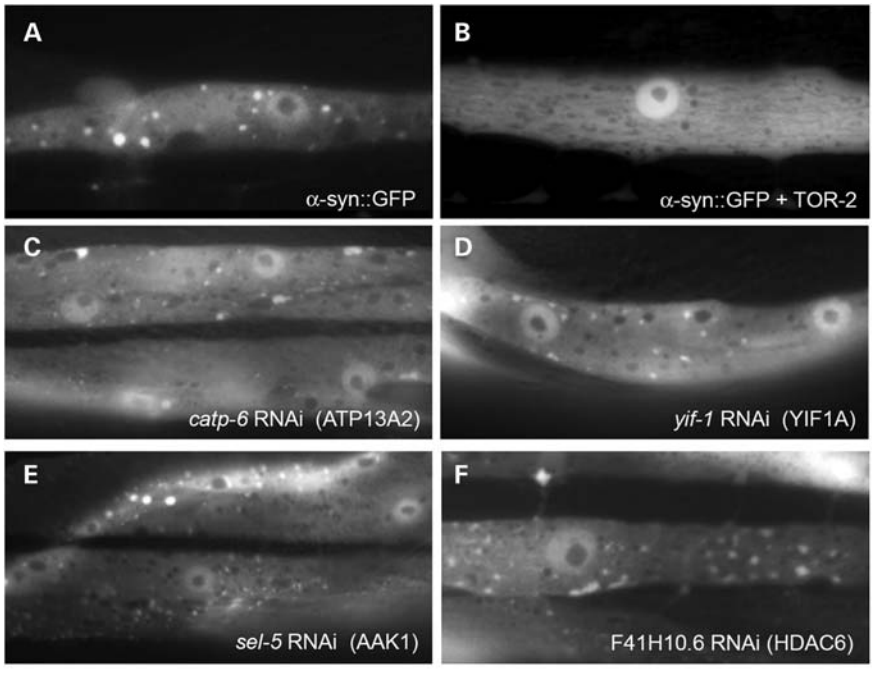

C. elegans gene ID	Description
C16D6.2	neuropeptide Y receptor Y1 (NPYIR)
F20B6.8a (*hpk-1*)	homeodomain interacting protein kinase 1 (HIPK1)
F35G12.3b (*sel-5*)	AP2 associated kinase 1 (AAK1)
K09G1.4 (*dop-2*)	coagulation factor II (thrombin) receptor (F2R)
R106.2	coagulation factor II (thrombin) receptor (F2R)
F41H10.6 (*hdac-6*)	histone deacetylase 6 (HDAC6)
Y37D8A.10 (*hpo-21*)	signal peptidase complex subunit 2 (SPCS2)
F57A8.2 (*yif-1*)	YIP1 interacting factor homolog A (YIF1A)

Figure 3. Knockdown of specific gene targets using RNAi enhances misfolding of α -syn in *C. elegans*. (**A**) Isogenic worms expressing the α -syn::green fluorescence protein (GFP) transgene alone in body wall muscle cells of *C. elegans* (P_{unc-54}::α-syn::GFP) display a misfolded protein as indicated by the GFP puncta. (**B**) In the presence of TOR-2 (P_{unc-54}::α-syn::GFP + P_{unc-54}::tor-2), a protein with chaperone activity, the misfolded α-syn protein is attenuated and puncta are no longer visible. (**C**) When worms expressing α-syn::GFP + TOR-2 are exposed to *catp-6* (ATP13A2) RNAi, the misfolded α-syn::GFP returns. (**D**–**F**) Misfolded α-syn::GFP also returns when worms expressing α-syn::GFP + TOR-2 are depleted, via RNAi, for specific candidate genes that interact with ATP13A2. Representative images of genes that are knocked down are displayed in this image [*yif-1* (D), *sel-5* (E) and F41H10.6 (F)]. The corresponding human orthologs are YIF1A, AAK1 and HDAC6, respectively. The listing below summarizes the ATP13A2 interactors that, when knocked down via RNAi, caused α-syn misfolding in *C. elegans* body wall muscle cells. The human orthologs corresponding to these eight interactors are also provided.

In order to further examine the link between α-syn and ATP13A2, we tested the ability of our ATP13A2 interactors to modify α-syn aggregation in *C. elegans.* We focused on 22 interactors that had well-defined worm orthologs and were available in the *C. elegans* RNA interference (RNAi) library (22). However, two of the 22 human candidates had two different worm orthologs, bringing the total number of gene candidates available for screening in *C. elegans* to 24 (Supplementary Material, Table S3). RNAi was used to knockdown each of the candidate genes, in duplicate, in *C. elegans* to examine whether depletion enhanced α-syn misfolding. This nematode model consists of overexpression of human α-syn fused to green fluorescence protein (GFP) at the C terminus, wherein the expression of this construct in the body wall muscle cells (P_{unc-54}::α-syn::GFP) of the animal (7) exhibits age-dependent α-syn misfolding in the cytoplasm (Fig. 3A). Moreover, the co-expression of a chaperone, TOR-2, reduces α-syn::GFP misfolding, wherein the majority of the muscle cells exhibit diffuse GFP (Fig. 3B). These animals provide a genetic background in which the enhancement of α-syn misfolding is easily visualized. Using this model, RNAi was conducted to knockdown the worm orthologs of 24 ATP13A2 interactor candidates. Depletion of *C. elegans catp-6* (ATP13A2) resulted in increased misfolding of α-syn, as described previously (8), and served as a positive control (Fig. 3C). The depletion of 8 of 24 candidate genes by RNAi also significantly enhanced α-syn misfolding (Fig. 3 table). Representative images of enhanced α-syn misfolding in worms expressing α-syn::GFP + TOR-2 with RNAi targeting candidate genes are shown in Figure 3D–F.

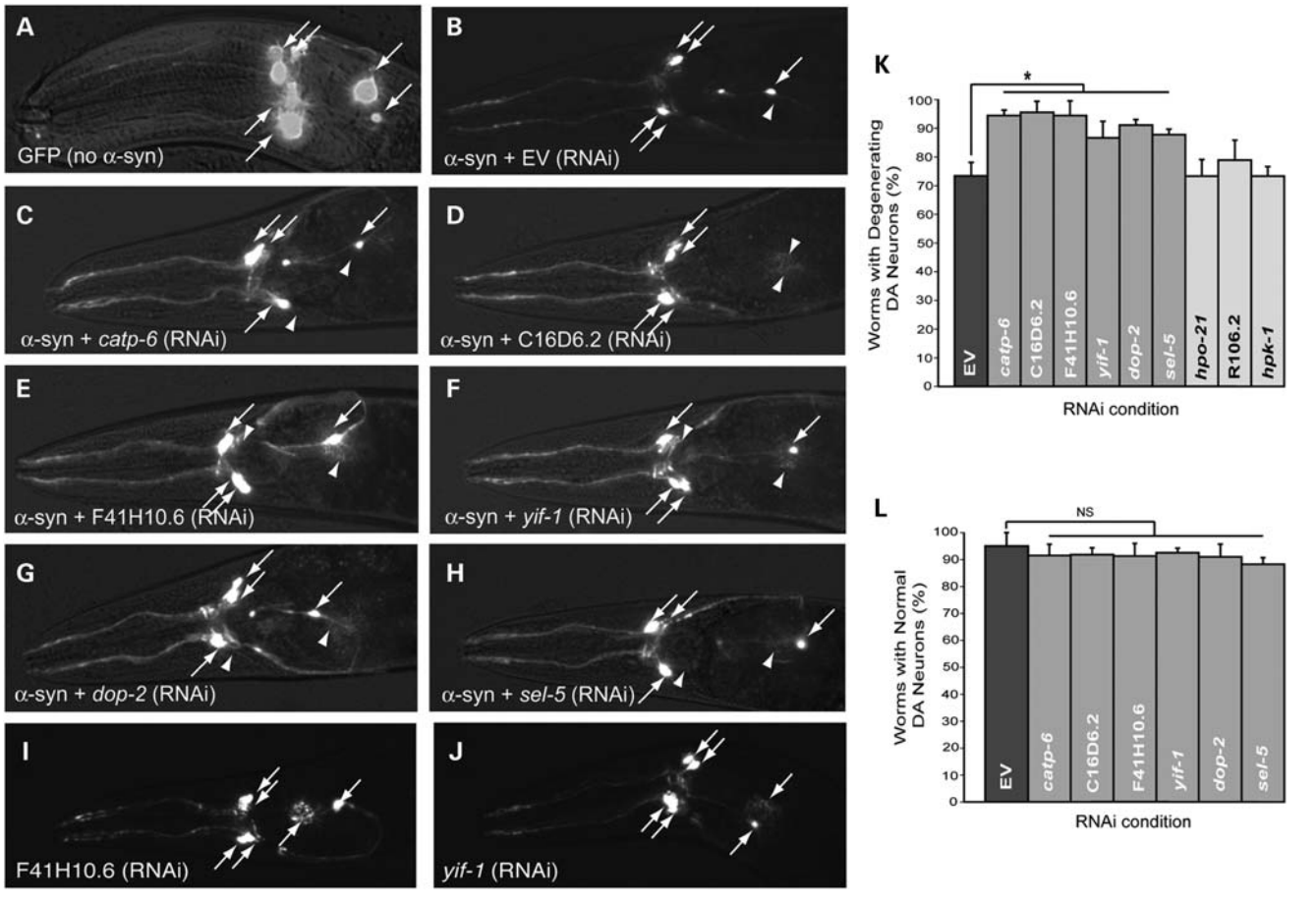

Figure 4. Deficiency of positive *catp-6* (ATP13A2) interactors enhances α-syn-induced DA neurodegeneration. (**A**) The anterior DA neurons of a *C. elegans* hermaphrodite are selectively illuminated using GFP driven from the DA transporter promoter (P_{dat-1}::GFP). The six cell bodies are indicated with arrows. (**B**) A representative worm co-expressing both GFP and α-syn in DA neurons displaying neurodegeneration. An arrowhead indicates the approximate location of a missing neuron. These worms were also treated with EV RNAi as a negative control. (**C**) A representative worm co-expressing GFP and α-syn in DA neurons, treated with the positive control, *catp-6*/ATP13A2 (RNAi), demonstrating enhanced neurodegeneration compared with EV (RNAi) where two neurons are missing in this representative animal (arrowheads). (**D**–**H**) Knockdown of five positive candidates also yielded significantly greater numbers of missing DA neurons compared with the EV control RNAi. These candidates are C16D6.2 (D), F41H10.6 (E), *yif-1* (F), *dop-2* (G) and *sel-5* (H). (**I** and **J**) Representative images of the DA neurons following the knockdown of F41H10.6 (HDAC6) and *yif-1* (YIF1A) in *C. elegans* in a background lacking α-syn (P_{dat-1}::GFP only), where the six anterior DA neurons remain intact, as indicated with arrows. (**K**) A graphical representation of the quantitative analysis of worm populations exhibiting enhanced α-syn-induced DA neurodegeneration upon the RNAi knockdown of positive ATP13A2 interactors. Populations of worms expressing α-syn with EV RNAi displayed 74% degeneration at the 6-day stage of development. The amount of degeneration is significantly enhanced to 94% when these worms are treated with *catp-6* RNAi, the positive control (ATP13A2). The five positive candidates showed similar significant levels of degeneration; these are C16D6.2, F41H10.6, *yif-1*, *dop-2* and *sel-5* ($^*P < 0.05$ by one-way ANOVA). The corresponding human orthologs are NPY1R, HDAC6, YIF1A, F2R and AAK, respectively. (**L**) The five candidates that enhanced α-syn-induced neurodegeneration in *C. elegans* were examined in the absence of α-syn for effects on neurodegeneration (P_{dat-1}::GFP only). None of the five positive candidates caused significant degeneration when knocked down compared with control RNAi (EV). Values are expressed as mean ± standard deviation (SD) from three independent replicates.

α-syn-induced dopaminergic neurodegeneration is enhanced when ATP13A2 interactors are depleted in *C. elegans*

Having discovered a set of ATP13A2 interactors that modify α-syn misfolding, we hypothesized that these eight candidates might also have an effect in the toxicity of dopamine (DA) neurons. We previously established that the overexpression of wild-type human α-syn cDNA under the control of a DA transport-specific promoter [P_{dat-1}:: α-syn+ P_{dat-1}::GFP] results in age- and dose-dependent degeneration of DA neurons in comparison to neurons expressing GFP alone (23) (Fig. 4A and B). By day 6 of adulthood most animals are missing at least one anterior DA neuron (Fig. 4B). We wanted to examine the eight positive candidates in this α-syn-induced degeneration model, via RNAi knockdown, to determine if candidate depletion would modulate the amount of degeneration. However, until recently, DA neurons in *C. elegans* have been notoriously refractive to RNAi, an experimental challenge that has limited the direct evaluation of genetic effectors of DA neurodegeneration by this otherwise powerful methodology (24). For RNAi silencing in neurons, we utilized a new method (25) where worms exhibited selective RNAi silencing pan-neuronally. These worms were crossed into our P_{dat-1}:: α-syn+ P_{dat-1}::GFP strain which allowed the impact of candidates knocked down via RNAi to be examined exclusively in the DA neurons.

An unequivocal advantage of *C. elegans* is that detailed quantitative analyses of neurons are achievable. There are precisely six DA neurons within the anterior region of the worm that consistently display degenerative characteristics. We examined worms for changes in the cell bodies as well as the neuronal processes for normal appearance versus degenerative changes (Fig. 4). Using the pan-neuronal, cell-specific RNAi strain, expressing α-syn+ GFP in the DA neurons, we knocked down the eight candidate genes and analyzed the DA neurons for degeneration. A total of 30 animals, in triplicate, were analyzed per RNAi condition, for a total of 90 animals per gene knockdown. This analysis examined the extent of neuronal damage within a population of individuals to determine what percentage of the worm population exhibited any neuronal degeneration (i.e. if even one of the six DA neurons was degenerating, the entire animal was considered as a mutant). This reporting method may be akin to the clinical situation wherein a patient (or worm or rat) is scored as affected or unaffected. When the empty vector (EV) control RNAi was examined, 74% of the worm population displayed degeneration at day 6 of development. Within the worm population treated with RNAi for the positive control, *catp-6*, 94% displayed enhanced neuron degeneration [Fig. 4C and K ($P < 0.05$ by one-way analysis of variance, ANOVA)]. This increase in α-syn toxicity resulting from the depletion of *catp-6* was consistent with the RNAi result obtained from the body wall muscle cells where the depletion of *catp-6* caused enhanced α-syn misfolding (Fig. 3C). These results were also complementary to those previously described where ATP13A2 overexpression rescued α-syn-induced DA neuron degeneration (8).

When worm populations were depleted for the gene products of the *catp-6* interactors, five of the eight candidates resulted in significant DA neurodegeneration. These candidates were C16D6.2 (96% degeneration), F41H10.6 (95%), *yif-1* (85%), *dop-2* (90%) and *sel-5* (88%). The corresponding human orthologs are NPY1R, HDAC6, YIF1A, F2R and AAK1, respectively [Fig. 4D–H and K ($P < 0.05$ by one-way ANOVA)]. From this analysis, three of the eight candidates did not significantly enhance the amount of DA neuron degeneration observed in worms expressing α-syn. These candidates were *hpo-21*, R106.2 and *hpk-1* (the corresponding human orthologs are SPCS2, F2R and HIPK1, respectively).

To determine if the five positive candidates were specific to α-syn-mediated DA neurodegeneration or if they represented a general effect on DA neuron toxicity, we examined the knockdown of these candidates in a background lacking α-syn. For this investigation, we utilized a pan-neuronal, cell-specific RNAi strain expressing GFP only in the DA neurons ($P_{dat\text{-}1}$::GFP only). Notably, DA neurodegeneration was not observed following the knockdown of any of these five candidates when α-syn was absent, indicating that these modifiers are indeed specific to α-syn (Fig. 4I, J and L).

The existence of ATP13A2 interactors that enhance α-syn aggregation and α-syn-induced neurodegeneration suggests an overlap of genetic networks between ATP13A2 and α-syn, further strengthening the connection between these two proteins. The modifiers of α-syn misfolding and neurotoxicity belong to groups responsible for ER and Golgi transport (YIF1A), clathrin-mediated vesicular transport (AAK1) and lysosomal fusion and degradation of aggregated proteins (HDAC6), suggesting the importance of these processes in α-syn-mediated toxicity.

DISCUSSION

In this study, we identified interacting partners of ATP13A2 using the MYTH technology that was developed to discover interactors of integral membrane proteins (14). These newly identified protein partners provide insights into the normal function of ATP13A2 as well as contribute to our understanding of loss of ATP13A2 function in disease. Collectively, these interactors suggest a putative role for ATP13A2 in vesicular trafficking and fusion. For example, one of the identified interactors, the cytosolic chaperone HSPA8, and its co-chaperone FKBP38 are implicated in ER-to-Golgi and plasma membrane trafficking (26). HSPA8 also functions as an ATPase in the uncoating of clathrin-coated vesicles during the transport of membrane components through the cell (27). Another example of a gene candidates identified in the screen that are involved in clathrin-dependent vesicular trafficking is the AAK1 and cyclin GAK (/auxilin 2) (28–30). Notably, AAK1 also impacts α-syn aggregation and α-syn-induced neurodegeneration in *C. elegans*.

Furthermore, VAMP2 (/synaptobrevin 2) is a component of SNARE (soluble *N*-ethylmalemide-sensitive factor activating protein receptor) complexes that play a role in membrane fusion during synaptic vesicle exocytosis (31,32). SYT11 is a member of the synaptotagmin family of transmembrane proteins (SYTs) that functions in calcium-dependent vesicular trafficking/fusion and lysosomal exocytosis. Synaptotagmin binds to SNAREs in Ca^{2+}-dependent manner and triggers membrane fusion machinery (32–34). These interactors suggest that, in addition to its presumable function as ion pump (12), ATP13A2 might be involved in membrane fusion. There are other examples of ATPases with this type of dual functionality such as V-ATPase that primarily functions as a proton pump and also interacts with VAMP2 that it is involved in SNARE-dependent membrane fusion (35). In another recent study, genome-wide screens were performed in yeast to define the cellular function of yeast homolog of ATP13A2 (Ypk9) and the mechanism by which Ypk9 protects cells from manganese toxicity (36). This work suggested that Ypk9 plays a role in vesicle-mediate transport and vacuolar fusion and organization, further supporting the notion that ATP13A2 regulates vesicular trafficking.

Recent data demonstrated that the overexpression of yeast ATP13A2 (Ypk9) rescued α-syn-mediated toxicity and α-syn-induced blockade of ER-Golgi vesicular trafficking (8). These data suggested that ATP13A2 may play a role in vesicular trafficking and indicated the involvement of this pathway in α-syn-mediated toxicity. The fact that the knockdown of ATP13A2 causes α-syn aggregation and toxicity in a *C. elegans* model of PD also indicated a genetic link between ATP13A2 and α-syn (7,8). Here, we extend these observations by demonstrating that a subset of interactors of ATP13A2 act as modifiers of α-syn aggregation and neurotoxicity in *C. elegans*. These interactors/modifiers further suggest a role for vesicular trafficking in α-syn-mediated toxicity. For

example, AAK1 regulates clathrin-mediated endocytosis (29), YIF1A cycles between ER and Golgi to maintain the structure of the Golgi apparatus (37) and its yeast homolog (Yip1p) is responsible for ER-to-Golgi transport and vesicular fusion (38,39).

We also identified HDAC6 as an interacting protein of ATP13A2 that modifies α-syn misfolding and DA neurodegeneration in *C. elegans*. These results are consistent with previous studies in a *Drosophila* model of PD, in which depletion of HDAC6 resulted in the accumulation of α-syn inclusions and loss of DA neurons (40). Interestingly, HDAC6 has previously been implicated in the clearance of aggregation–prone proteins through autophagy, by recruiting and transporting aggresomes via the microtubule network and the dynein motor complex (41,42). HDAC6 also mediates F-actin polymerization, which provides a platform for the fusion of autophagosomes and lysosomes (43). Taken together, the interaction of HDAC6 with ATP13A2 suggests the involvement of ATP13A2 in the lysosomal degradation pathway and emphasizes the importance of protein clearance in mediating α-syn aggregation and toxicity.

The identification of genetic forms of PD resulting from multiplications of the wild-type α-syn gene (44) or missense mutations of α-syn (45) demonstrates that subtle changes in levels of this protein correlate with clinical presentation and identify the clearance of α-syn as a key therapeutic target. To this end, we and others have previously shown that impaired clearance of α-syn via the lysosomal pathway results in accumulation of toxic α-syn moieties, and consequently, neurodegeneration (46,47). Therefore, it can be hypothesized that loss of normal ATP13A2 function may contribute to lysosomal dysfunction and accumulation of α-syn, with detrimental consequences for neuron survival. This conclusion is at least in part supported by our finding that loss of ATP13A2 function results in α-syn-dependent degeneration of dopaminergic neurons (Fig. 4).

In conclusion, our data reveal that ATP13A2 plays a role in vesicular trafficking under physiological conditions and that disruption of these pathways contribute to α-syn-mediated toxicity. While further studies will be required to define the precise contribution of ATP13A2 to lysosome-associated neuroprotection and α-syn clearance, these results provide a platform for further mechanistic studies of biological function of ATP13A2, and its role in the pathogenesis of synucleinopathies.

MATERIALS AND METHODS

MYTH screen

Design and validation of the bait construct

The cDNA of full-length wild-type ATP13A2 (bait) was cloned into the vector pTMBV-MFα-Cub-TF by *in vivo* recombination in yeast strain THY.AP4 (MATa leu2-3,112 ura3-52 trp1-289lexA::HIS3 lexA::ADE2 lexA::lacZ) [detailed protocols in Snider *et al*. (15) and Iyer *et al*. (17)]. Signal sequence of yeast α-mating pheromone precursor (MFα) was added to the vector to facilitate insertion of human ATP13A2-Cub-TF into a yeast membrane. After the pTMBV-MFα-ATP13A2-Cub-TF sequence had been confirmed, expression, correct insertion of the fused protein into the membrane and non-self-activation of reporter genes were verified with 'NubG/I test' as previously described in detail (15). This assay was also used to select the optimal concentration of 3-amino-1,2,4-triazole (3-AT), a competitive inhibitor of HIS3 gene, to suppress background growth.

Screen for ATP13A2 interactors and bait dependency test

Yeast strain THY.AP4 containing pTMBV-MFα-ATP13A2-Cub-TF construct was transformed with human brain cDNA library (DualSystems Biotech Inc.) (preys) fused to the 3′ end of NubG moiety (NubG-prey orientation) by the lithium acetate protocol (48). The library has an average insert size of ∼1.5 kb and complexity of $\sim 2 \times 10^6$ independent clones (DualSystems Biotech Inc.). The total number of transformants in this screen was of around 4×10^6. Four hundred and eighty colonies were selected on SD-Leu-Trp-Ade-His + X-gal plates supplemented with 10 mM 3-AT. Plasmids from these yeast colonies were isolated by the zymolase method (17) and amplified in *Escherichia coli* XL10 gold with a standard protocol (49). To assay the specificity of the interaction, 480 selected prey plasmids were transformed back into THY.AP4 yeast strains expressing ATP13A2-Cub-TF (bait) and artificial bait MFα-CD4-Cub-TF (MFα signal sequence, the single-pass transmembrane domain of human T-cell surface glycoprotein CD4 and a Cub-TF tag). Since MFα-CD4-Cub-TF contains minimal extraneous sequence in addition to the tag, it does not interact with other proteins. Forty-three preys that activated ADE2/HIS3/*lac*Z reporter genes in yeast-bearing ATP13A2-Cub-TF but did not grow when co-expressed with artificial bait CD4-Cub-TF were sequenced and further analyzed.

Co-immunoprecipitation

HEK293FT cells were co-transfected with plasmids expressing V5-ATP13A2, FLAG-HDAC6, FLAG-NIX, enhanced green fluorescence protein (EGFP)-SYT11, EGFP-GAK, EGFP-AAK1, hemagglutinin (HA)-YIF1A and EGFP-HSPA8 (constructs were generously provided by Christian Kubisch, Tso-Pang Yao, Ivana Novak, Stefan Pulst, Lois Green, Sean Conner and Hiro Nakamura, respectively; HSPA8 construct was purchased from Addgen Inc.). Cells were lysed by incubation for 30 min at 4°C on a rocking platform in lysis buffer [50 mM 4-(2-hydroxyethyl)-1-piperazineethanesulfonic acid, 150 mM NaCl, 1 mM 2,2′,2″,2‴-(ethane-1,2-diyldinitrilo) tetraacetic acid, 1 mM ethylene glycol-bis(2-aminoethylether)-N,N,N′,N′-tetraacetic acid, 10% glycerol, 1% Triton X-100, 25 mM NaF, 10 μM $ZnCl_2$ (pH 7.5)] with protease inhibitor cocktail (Complete Mini, Roche Applied Science). To remove the insoluble fraction, collected cell lysates were centrifuged at 20 000*g* for 20 min. Supernatants were pre-cleared with protein A-Sepharose beads (Santa Cruz Biotechnology) for 1 h, incubated with V5 antibody (Invitrogen) overnight at 4°C and with protein A-Sepharose beads for 2 h. Proteins were detected on sodium dodecyl sulfate-polyacrylamide gel electrophoresis using antibodies to FLAG, EGFP, HA and V5 tags.

Bioinformatic analysis

Physical protein interactions were obtained from two sources. First, the Interologous Interaction Database (I2D, version 1.71) (50) was queried with Entrez Gene IDs for the bait ATP13A2 and 43 hits to extract a network of interacting proteins involving the screen hits. Second, tab-delimited interaction files were downloaded from BioGRID (v3.1) (51) and parsed to identify proteins known to interact with the screen hits. The network of MYTH hits plus known and predicted interaction were visualized using the NAViGaTOR graph visualization software (v2.2.1) (52). Edges, which represent physical protein–protein interactions, were colored according to the interaction source. Node color represents the functional category each gene was manually assigned to, based on its GO annotations. Enrichment for GO terms was performed using the DAVID functional annotation tool (v6.7; http://david.abcc.ncifcrf.gov/). GO_FAT categories comprising a more informative set of GO terms were used for enrichment of the GO Biological Process, Molecular Function and Cellular Compartment trees.

Caenorhabditis elegans strains

Nematodes were maintained following the standard procedures (53). Strain UA50 (baInl3, [P_{unc-54}::α-syn::gfp, P_{unc-54}::tor-2, rol-6 (su1006)]) was generated as described (23). Strain TU3401 (uIs69, [pCFJ90 (P_{myo-2}::mCherry), $P_{unc-119}$::sid-1]; sid-1(pk3321)), a gift from Martin Chalfie (25), was crossed to UA44 (baIn11, [P_{dat-1}:: α-syn, P_{dat-1}::gfp]) to generate UA197 (uIs69, [pCFJ90 (P_{myo-2}:: mCherry), $P_{unc-119}$::sid-1]; sid-1(pk3321); baIn11, [P_{dat-1}:: α-syn, P_{dat-1}::gfp]). Strain UA228 (uIs69, [pCFJ90 (P_{myo-2}:: mCherry)]; vtIs7, [P_{dat-1}::gfp]) was generated by crossing TU3401 with BY250 (vtIs7, [P_{dat-1}::gfp]) (a gift from Randy Blakely, Vanderbilt University).

Caenorhabditis elegans experiments

For α-syn misfolding studies in body wall muscles, RNAi was conducted as described (7) by feeding UA50 worms with RNAi clones (Geneservice, Cambridge, UK) targeting the worm orthologs of positive candidates from ATP13A2 MYTH screen with the following modification. Worms were grown on RNAi bacteria for an additional generation and then analyzed for α-syn misfolding at young adult stage (day 4; Fig. 3). Analysis was performed in duplicate, and candidates were scored as positive if RNAi significantly enhanced misfolding (80% of worms exhibited increased size and quantity of α-syn aggregates).

Likewise, for neurodegeneration assay in DA neurons, RNAi was conducted by feeding UA197 and UA228 worms with RNAi clones targeting the worm orthologs of ATP13A2 and the positive candidates from the α-syn misfolding screen with the following modification. UA197 worms were analyzed for α-syn-induced DA neurodegeneration on Day 6 (Fig. 4A–I) and UA228 worms were analyzed for DA neuron degeneration on Day 7 (Fig. 4J–L). A total of 90 animals for each gene were analyzed (3 trials of 30 animals/trial). Worms were considered wild-type when all four cephalic and both anterior deirid neurons were intact and had no visible signs of degeneration. If a worm displayed at least one degenerative change (dendrite or axon loss, cell body loss), the animal was scored as exhibiting degenerating neurons (7,23). For statistical analysis, quantitative data were displayed as arithmetic means ± SD in triplicate, and the one-way ANOVA followed by the Dunnett's multiple comparison test ($P < 0.05$) was used to examine significance (GraphPad Prism Software, version 5.0). All images were taken by fluorescence microscopy (7) on the same day of analysis.

SUPPLEMENTARY MATERIAL

Supplementary Material is available at *HMG* online.

ACKNOWLEDGEMENTS

We thank Drs John Graziotto, Saranya Kittanakom and other members of the Krainc, Stagljar and Caldwell laboratories for helpful suggestions and discussions. Additional thanks to Drs Marty Chalfie and Randy Blakeley for transgenic nematode strains. Special thanks to Dr Adam Harrington for assistance in generating the α-syn neuron-specific RNAi strain.

Conflict of Interest statement. None declared.

FUNDING

This work was supported by National Institutes of Health (R01NS051303 to D.K. and R15NS075684 to G.A.C.). The research in the Stagljar lab is supported by grants from the Canadian Foundation for Innovation (CFI), the Canadian Institutes of Health Research (CIHR), the Canadian Cancer Society Research Institute (CCSRI), the Heart and Stroke Foundation, the Cystic Fibrosis Foundation, the Ontario Genomics Institute, Natural Sciences and Engineering Research Council of Canada (NSERC), and Novartis.

REFERENCES

1. Schultz, M.L., Tecedor, L., Chang, M. and Davidson, B.L. (2011) Clarifying lysosomal storage diseases. *Trends Neurosci.*, **34**, 401–410.
2. Nixon, R.A., Yang, D.-S. and Lee, J.-H. (2008) Neurodegenerative lysosomal disorders: continuum from development to late age. *Autophagy*, **4**, 590–599.
3. Zhang, L., Sheng, R. and Qin, Z. (2009) The lysosome and neurodegenerative diseases. *Acta Biochim. Biophys. Sin. (Shanghai)*, **41**, 437–445.
4. Ramirez, A., Heimbach, A., Gründemann, J., Stiller, B., Hampshire, D., Cid, L.P., Goebel, I., Mubaidin, A.F., Wriekat, A.-L., Roeper, J. *et al.* (2006) Hereditary parkinsonism with dementia is caused by mutations in ATP13A2, encoding a lysosomal type 5 P-type ATPase. *Nat. Genet.*, **38**, 1184–1191.
5. Di Fonzo, A., Chien, H.F., Socal, M., Giraudo, S., Tassorelli, C., Iliceto, G., Fabbrini, G., Marconi, R., Fincati, E., Abbruzzese, G. *et al.* (2007) ATP13A2 missense mutations in juvenile parkinsonism and young onset Parkinson disease. *Neurology*, **68**, 1557–1562.
6. Park, J.-S., Mehta, P., Cooper, A.A., Veivers, D., Heimbach, A., Stiller, B., Kubisch, C., Fung, V.S., Krainc, D., Mackay-Sim, A. *et al.* (2011) Pathogenic effects of novel mutations in the P-type ATPase ATP13A2 (PARK9) causing Kufor-Rakeb syndrome, a form of early-onset parkinsonism. *Hum. Mutat.*, **32**, 956–964.
7. Hamamichi, S., Rivas, R.N., Knight, A.L., Cao, S., Caldwell, K.A. and Caldwell, G.A. (2008) Hypothesis-based RNAi screening identifies neuroprotective genes in a Parkinson's disease model. *Proc. Natl Acad. Sci. USA*, **105**, 728–733.

8. Gitler, A.D., Chesi, A., Geddie, M.L., Strathearn, K.E., Hamamichi, S., Hill, K.J., Caldwell, K.A., Caldwell, G.A., Cooper, A.A., Rochet, J.-C. *et al.* (2009) Alpha-synuclein is part of a diverse and highly conserved interaction network that includes PARK9 and manganese toxicity. *Nat. Genet.*, **41**, 308–315.
9. Yeger-Lotem, E., Riva, L., Su, L.J., Gitler, A.D., Cashikar, A.G., King, O.D., Auluck, P.K., Geddie, M.L., Valastyan, J.S., Karger, D.R. *et al.* (2009) Bridging high- throughput genetic and transcriptional data reveals cellular responses to alpha-synuclein toxicity. *Nat. Genet.*, **41**, 316–323.
10. Gusdon, A.M., Zhu, J., Van Houten, B. and Chu, C.T. (2011) ATP13A2 regulates mitochondrial bioenergetics through macroautophagy. *Neurobiol. Dis.*, **45**, 962–972.
11. Grünewald, A., Arns, B., Seibler, P., Rakovic, A., Münchau, A., Ramirez, A., Sue, C.M. and Klein, C. (2012) ATP13A2 mutations impair mitochondrial function in fibroblasts from patients with Kufor-Rakeb syndrome. *Neurobiol. Aging*, in press.
12. Kühlbrandt, W. (2004) Biology, structure and mechanism of P-type ATPases. *Nat. Rev. Mol. Cell Biol.*, **5**, 282–295.
13. Tan, J., Zhang, T., Jiang, L., Chi, J., Hu, D., Pan, Q., Wang, D. and Zhang, Z. (2011) Regulation of intracellular manganese homeostasis by Kufor-Rakeb syndrome-associated ATP13A2 protein. *J. Biol. Chem.*, **286**, 29654–29662.
14. Stagljar, I., Korostensky, C., Johnsson, N. and te Heesen, S. (1998) A genetic system based on split-ubiquitin for the analysis of interactions between membrane proteins in vivo. *Proc. Natl Acad. Sci. USA*, **95**, 5187–5192.
15. Snider, J., Kittanakom, S., Damjanovic, D., Curak, J., Wong, V. and Stagljar, I. (2010) Detecting interactions with membrane proteins using a membrane two-hybrid assay in yeast. *Nat. Protoc.*, **5**, 1281–1293.
16. Johnsson, N. and Varshavsky, A. (1994) Split ubiquitin as a sensor of protein interactions in vivo. *Proc. Natl Acad. Sci. USA*, **91**, 10340–10344.
17. Iyer, K., Bürkle, L., Auerbach, D., Thaminy, S., Dinkel, M., Engels, K. and Stagljar, I. (2005) Utilizing the split-ubiquitin membrane yeast two-hybrid system to identify protein-protein interactions of integral membrane proteins. *Sci. STKE*, **2005**, pl3.
18. Petschnigg, J., Wong, V., Snider, J. and Stagljar, I. (2012) Investigation of membrane protein interactions using the split-ubiquitin membrane yeast two-hybrid system. *Methods Mol. Biol.*, **812**, 225–244.
19. Ashburner, M., Ball, C.A., Blake, J.A., Botstein, D., Butler, H., Cherry, J.M., Davis, A.P., Dolinski, K., Dwight, S.S., Eppig, J.T. *et al.* (2000) Gene ontology: tool for the unification of biology. The Gene Ontology Consortium. *Nat. Genet.*, **25**, 25–29.
20. Huang, D.W., Sherman, B.T. and Lempicki, R.A. (2009) Systematic and integrative analysis of large gene lists using DAVID bioinformatics resources. *Nat. Protoc.*, **4**, 44–57.
21. Ramonet, D., Podhajska, A., Stafa, K., Sonnay, S., Trancikova, A., Tsika, E., Pletnikova, O., Troncoso, J.C., Glauser, L. and Moore, D.J. (2012) PARK9-associated ATP13A2 localizes to intracellular acidic vesicles and regulates cation homeostasis and neuronal integrity. *Hum. Mol. Genet.*, **21**, 1725–1743.
22. Kamath, R.S. and Ahringer, J. (2003) Genome-wide RNAi screening in *Caenorhabditis elegans*. *Methods*, **30**, 313–321.
23. Cao, S., Gelwix, C.C., Caldwell, K.A. and Caldwell, G.A. (2005) Torsin-mediated protection from cellular stress in the dopaminergic neurons of *Caenorhabditis elegans*. *J. Neurosci.*, **25**, 3801–3812.
24. Asikainen, S., Vartiainen, S., Lakso, M., Nass, R. and Wong, G. (2005) Selective sensitivity of *Caenorhabditis elegans* neurons to RNA interference. *Neuroreport*, **16**, 1995–1999.
25. Calixto, A., Chelur, D., Topalidou, I., Chen, X. and Chalfie, M. (2010) Enhanced neuronal RNAi in C. elegans using SID-1. *Nat. Methods*, **7**, 554–559.
26. Walker, V.E., Atanasiu, R., Lam, H. and Shrier, A. (2007) Co-chaperone FKBP38 promotes HERG trafficking. *J. Biol. Chem.*, **282**, 23509–23516.
27. Schlossman, D.M., Schmid, S.L., Braell, W.A. and Rothman, J.E. (1984) An enzyme that removes clathrin coats: purification of an uncoating ATPase. *J. Cell Biol.*, **99**, 723–733.
28. Eisenberg, E. and Greene, L.E. (2007) Multiple roles of auxilin and hsc70 in clathrin-mediated endocytosis. *Traffic*, **8**, 640–646.
29. Conner, S.D. and Schmid, S.L. (2002) Identification of an adaptor-associated kinase, AAK1, as a regulator of clathrin-mediated endocytosis. *J. Cell Biol.*, **156**, 921–929.
30. Lee, D.-W., Zhao, X., Yim, Y.-I., Eisenberg, E. and Greene, L.E. (2008) Essential role of cyclin-G-associated kinase (Auxilin-2) in developing and mature mice. *Mol. Biol. Cell*, **19**, 2766–2776.
31. Duman, J.G. and Forte, J.G. (2003) What is the role of SNARE proteins in membrane fusion? *Am. J. Physiol. Cell Physiol.*, **285**, C237–C249.
32. Südhof, T.C. and Rizo, J. (2011) Synaptic vesicle exocytosis. *Cold Spring Harb. Perspect. Biol.* **3**, a005637.
33. Bai, J., Wang, C.-T., Richards, D.A., Jackson, M.B. and Chapman, E.R. (2004) Fusion pore dynamics are regulated by synaptotagmin*t-SNARE interactions. *Neuron*, **41**, 929–942.
34. Sudhof, T.C. (2004) The synaptic vesicle cycle. *Annu. Rev. Neurosci.*, **27**, 509–547.
35. El Far, O. and Seagar, M. (2011) A role for V-ATPase subunits in synaptic vesicle fusion? *J. Neurochem.*, **117**, 603–612.
36. Chesi, A., Kilaru, A., Fang, X., Cooper, A.A. and Gitler, A.D. (2012) The role of the Parkinson's disease gene PARK9 in essential cellular pathways and the manganese homeostasis network in yeast. *PLoS One*, **7**, e34178.
37. Yoshida, Y., Suzuki, K., Yamamoto, A., Sakai, N., Bando, M., Tanimoto, K., Yamaguchi, Y., Sakaguchi, T., Akhter, H., Fujii, G. *et al.* (2008) YIPF5 and YIF1A recycle between the ER and the Golgi apparatus and are involved in the maintenance of the Golgi structure. *Exp. Cell Res.*, **314**, 3427–3443.
38. Matern, H., Yang, X., Andrulis, E., Sternglanz, R., Trepte, H.H. and Gallwitz, D. (2000) A novel Golgi membrane protein is part of a GTPase-binding protein complex involved in vesicle targeting. *EMBO J.*, **19**, 4485–4492.
39. Barrowman, J., Wang, W., Zhang, Y. and Ferro-Novick, S. (2003) The Yip1p.Yif1p complex is required for the fusion competence of endoplasmic reticulum-derived vesicles. *J. Biol. Chem.*, **278**, 19878–19884.
40. Du, G., Liu, X., Chen, X., Song, M., Yan, Y., Jiao, R. and Wang, C.-C. (2010) Drosophila histone deacetylase 6 protects dopaminergic neurons against {alpha}-synuclein toxicity by promoting inclusion formation. *Mol. Biol. Cell*, **21**, 2128–2137.
41. Kawaguchi, Y., Kovacs, J.J., McLaurin, A., Vance, J.M., Ito, A. and Yao, T.P. (2003) The deacetylase HDAC6 regulates aggresome formation and cell viability in response to misfolded protein stress. *Cell*, **115**, 727–738.
42. Pandey, U.B., Nie, Z., Batlevi, Y., McCray, B.A., Ritson, G.P., Nedelsky, N.B., Schwartz, S.L., DiProspero, N.A., Knight, M.A., Schuldiner, O. *et al.* (2007) HDAC6 rescues neurodegeneration and provides an essential link between autophagy and the UPS. *Nature*, **447**, 859–863.
43. Lee, J.-Y., Koga, H., Kawaguchi, Y., Tang, W., Wong, E., Gao, Y.-S., Pandey, U.B., Kaushik, S., Tresse, E., Lu, J. *et al.* (2010) HDAC6 controls autophagosome maturation essential for ubiquitin-selective quality-control autophagy. *EMBO J.*, **29**, 969–980.
44. Devine, M.J., Gwinn, K., Singleton, A. and Hardy, J. (2011) Parkinson's disease and α-synuclein expression. *Mov. Disord.*, **26**, 2160–2168.
45. Goedert, M. (2001) Alpha-synuclein and neurodegenerative diseases. *Nat. Rev. Neurosci.*, **2**, 492–501.
46. Mazzulli, J.R., Xu, Y.-H., Sun, Y., Knight, A.L., McLean, P.J., Caldwell, G.A., Sidransky, E., Grabowski, G.A. and Krainc, D. (2011) Gaucher disease glucocerebrosidase and α-synuclein form a bidirectional pathogenic loop in synucleinopathies. *Cell*, **146**, 37–52.
47. Ebrahimi-Fakhari, D., Cantuti-Castelvetri, I., Fan, Z., Rockenstein, E., Masliah, E., Hyman, B.T., McLean, P.J. and Unni, V.K. (2011) Distinct roles in vivo for the ubiquitin-proteasome system and the autophagy-lysosomal pathway in the degradation of α-synuclein. *J. Neurosci.*, **31**, 14508–14520.
48. Gietz, R.D. and Schiestl, R.H. (2007) High-efficiency yeast transformation using the LiAc/SS carrier DNA/PEG method. *Nat. Protoc.*, **2**, 31–34.
49. Inoue, H., Nojima, H. and Okayama, H. (1990) High efficiency transformation of *Escherichia coli* with plasmids. *Gene*, **96**, 23–28.
50. Brown, K.R. and Jurisica, I. (2005) Online predicted human interaction database. *Bioinformatics*, **21**, 2076–2082.
51. Stark, C., Breitkreutz, B.-J., Reguly, T., Boucher, L., Breitkreutz, A. and Tyers, M. (2006) BioGRID: a general repository for interaction datasets. *Nucleic Acids Res.*, **34**, D535–D539.
52. Brown, K.R., Otasek, D., Ali, M., McGuffin, M.J., Xie, W., Devani, B., van Toch, I.L. and Jurisica, I. (2009) NAViGaTOR: Network Analysis, Visualization and Graphing Toronto. *Bioinformatics*, **25**, 3327–3329.
53. Brenner, S. (1974) The genetics of *Caenorhabditis elegans*. *Genetics*, **77**, 71–94.